J. Fluid Mech. (1980), *vol.* 101, *part* 1, *pp.* 159–178
Printed in Great Britain

Full-coverage film cooling. Part 2. Prediction of the recovery-region hydrodynamics

By S. YAVUZKURT, R. J. MOFFAT AND W. M. KAYS
Mechanical Engineering Department, Stanford University, CA 94305

(Received 31 January 1979 and in revised form 29 January 1980)

Hydrodynamic data are reported in the companion paper (Yavuzkurt, Moffat & Kays 1980) for a full-coverage film-cooling situation, both for the blown and the recovery regions. Values of the mean velocity, the turbulent shear stress, and the turbulence kinetic energy were measured at various locations, both within the blown region and in the recovery region. The present paper is concerned with an analysis of the recovery region only. Examination of the data suggested that the recovery-region hydrodynamics could be modelled by considering that a new boundary layer began to grow immediately after the cessation of blowing. Distributions of the Prandtl mixing length were calculated from the data using the measured values of mean velocity and turbulent shear stresses. The mixing-length distributions were consistent with the notion of a dual boundary-layer structure in the recovery region. The measured distributions of mixing length were described by using a piecewise continuous but heuristic fit, consistent with the concept of two quasi-independent layers suggested by the general appearance of the data. This distribution of mixing length, together with a set of otherwise normal constants for a two-dimensional boundary layer, successfully predicted all of the observed features of the flow. The program used in these predictions contains a one-equation model of turbulence, using turbulence kinetic energy with an algebraic mixing length. The program is a two-dimensional, finite-difference program capable of predicting the mean velocity and turbulence kinetic energy profiles based upon initial values, boundary conditions, and a closure condition.

1. Introduction

Most of the work in the literature at the present time concentrates upon measurements or predictions of either the film-cooling effectiveness or the surface heat transfer coefficient within the full-coverage region. It has been found generally successful to use two-dimensional boundary-layer predictor programs with an augmented mixing-length concept to predict the general features of full-coverage film-cooling heat transfer, again within the full-coverage region. Little has been done to investigate the recovery region, defined as the region of impermeable plate downstream of an array of film-cooling holes. It is this region which is the subject of the present work.

Crawford, Kays & Moffat (1976) give a summary of analytical work in the field of full-coverage film cooling. Goldstein *et al.* (1969) and Ericksen, Eckert & Goldstein (1971) used superposition of film-effectiveness data from individual jets to predict full-coverage effectiveness, modelling injection as a point heat source. Mayle & Camarata (1975) developed an improved superposition method to predict their full-coverage data. Pai & Whitelaw (1971) and Patankar, Rastogi & Whitelaw (1973)

0022-1120/80/4535-2320 $02.00

investigated the prediction of wall temperature and effectiveness downstream of two- and three-dimensional film-cooling slots. For the two-dimensional slot injection, the boundary-layer equations were used together with an augmented mixing-length model to represent the effect of injection. For three-dimensional injection, the Navier–Stokes equations were solved numerically by reducing them to elliptic form in the lateral plane and to parabolic form in the streamwise direction.

Herring (1975) used a finite-difference method for predicting the flow over a full-coverage film-cooled surface. Lateral averaging in the full-coverage region was invoked to justify using two-dimensional boundary-layer equations. Terms arising from the spanwise averaging were obtained from consideration of the jet/boundary-layer interaction. Predicted velocity profiles were reported but showed some problems in the initial regions of injection near the wall.

Choe, Kays & Moffat (1975) developed a finite-difference method for predicting heat transfer with full-coverage film cooling, solving the two-dimensional boundary-layer equations. (These equations have a form similar to those given by Herring 1975.) Choe *et al.* (1975) used the concept of local averaging, with a different model for the injection process, the nonlinear terms, and augmented turbulent mixing. Using an augmented mixing length in a one-equation model for turbulence, he successfully predicted most of their Stanton number data for low and moderate blowing in the full-coverage region. The predictions in the recovery region and for high blowing were less accurate.

Crawford *et al.* (1976) repeated the conditions covered by Choe *et al.*(1975), using a different full-coverage surface, however: 30° slant-hole injection with a staggered array of holes. With the injection temperature equal to the wall temperature, the Stanton number decreased below the normal flat-plate value and reached a minimum at a blowing ratio, M, of 0·4. Higher M caused an increase in the Stanton number. For the recovery region, downstream of the five-diameter hole array, two distinct data trends were observed. For low M the Stanton number began to recover immediately from the effects of blowing, while for high M the Stanton number either remained constant or dropped throughout the recovery region. This latter behaviour suggested that important differences might exist in the recovery-region hydrodynamics.

Experimental data concerning heat transfer in the recovery region show that the current boundary-layer predictor programs do not well handle this region. In view of the probable importance of interrupted film cooling (i.e. an array of holes followed by a blank surface, followed by an additional array of holes), it seems important to understand the recovery region behaviour more thoroughly. In particular, it would be desirable to be able to deal with the recovery region for the conventional two-dimensional boundary-layer predictor program.

The objective of the present study was to adapt a one-equation model of turbulence for the prediction of the hydrodynamic behaviour within the recovery region, based upon experimental data concerning the hydrodynamic structure. The experimental input upon which the present model is based was taken from the work of Yavuzkurt *et al.* (1977), described in the companion paper (Yavuzkurt *et al.* 1980; hereinafter referred to as I).

The present paper begins with the data sets describing mean velocity, TKE, shear stress, and mixing length reported in I. For details of the apparatus and the experimental methods used, readers are referred to I and the thesis of Yavuzkurt *et al.* (1977).

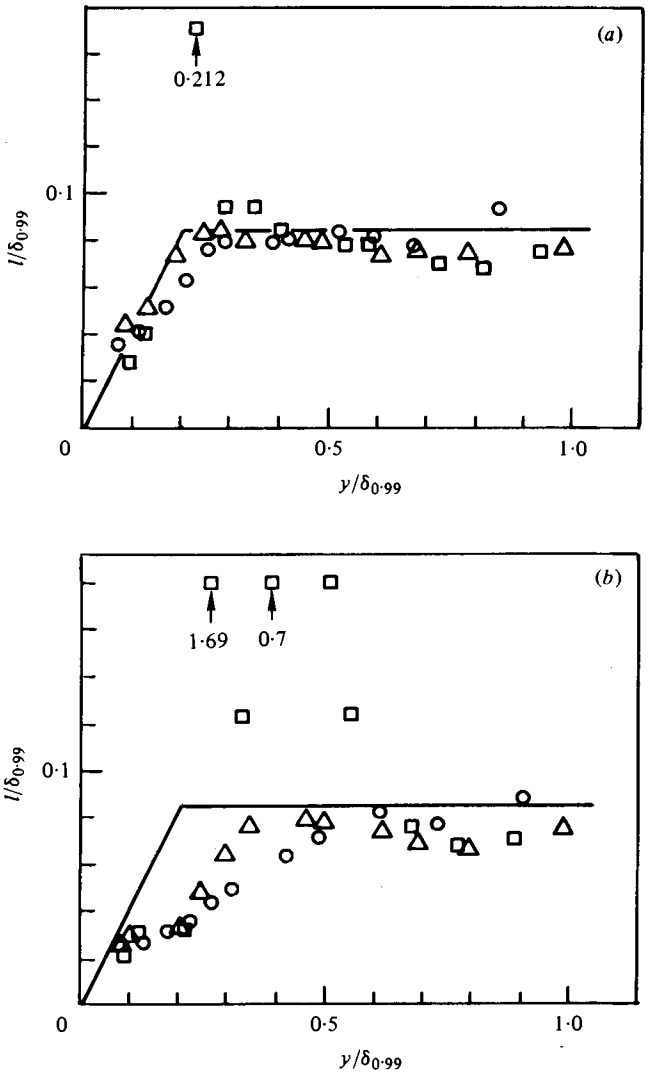

FIGURE 1. Mixing-length distribution in the recovery region (*a*) for $M = 0{\cdot}4$ and (*b*) for $M = 0{\cdot}9$. ——, flat plate; □, $x = 188$; △, $x = 214$; ○, $x = 256$.

Figures 1 (*a*, *b*) are reproduced from I, and show the distributions of mixing-length values calculated from the recovery region data sets. These were calculated using the spanwise-averaged mean velocity profiles and the spanwise-averaged turbulent shear stresses, and serve as the basis for the modelling of the turbulence processes within the recovery region.

The 'hump' in the inner region of the mixing-length distribution for $M = 0{\cdot}9$ (figure 1*b*) suggested the use of a dual boundary-layer model: an inner layer and an outer layer. Nothing in subsequent work contradicted this notion, and calculations based upon it have proved quite successful in predicting recovery region behaviour.

Prediction of streamwise evolution of the recovery region boundary layers requires initial conditions. These were taken from the data sets of I, using the mean velocity and turbulence kinetic energy distributions at the upstream end of the recovery region.

In the following sections, the theory is evolved, the model described, and results of the modelling presented.

2. General characteristics of a one-equation model of turbulence

It was desired to develop a one-equation turbulence model (TKE and mixing length) for use in an existing two-dimensional boundary-layer program, STAN5 (Crawford & Kays 1975). The one-equation concept requires an algebraic equation for the mixing length. Mixing length profiles were first obtained from the experimental profiles ($\overline{u'v'}$ and $\overline{U}$) using purely empirical curve fits to model the behaviour. This piecewise model was inserted into STAN5, and it was demonstrated that all important features of the data were well represented. Each region in the mixing-length profile was then interpreted physically and alternative, physically based equations identified. This procedure showed that all the important features of the recovery region hydrodynamics could be satisfactorily explained by postulating a two-dimensional boundary layer growing inside the thicker initial boundary layer. The following sections present the details of these steps.

2.1. *Equations to be solved*

The following equations must be solved to obtain mean velocity and turbulence kinetic energy (TKE) profiles. For a two-dimensional, turbulent boundary layer under isothermal conditions, at ambient temperatures and low speeds, at a constant free-stream velocity and without any external body forces:

$$\frac{\partial \overline{U}}{\partial x}+\frac{\partial \overline{V}}{\partial y}=0 \quad \text{continuity;} \tag{1}$$

$$\rho\overline{U}\frac{\partial \overline{U}}{\partial x}+\rho\overline{V}\frac{\partial \overline{U}}{\partial y}=\frac{\partial}{\partial y}\left(\mu\frac{\partial \overline{U}}{\partial y}-\rho\overline{u'v'}\right) \quad x \text{ momentum;} \tag{2}$$

$$\rho\overline{U}\frac{\partial(\frac{1}{2}q^2)}{\partial x}+\rho\overline{V}\frac{\partial(\frac{1}{2}q^2)}{\partial y}=\underbrace{-\rho\overline{u'v'}\frac{\partial \overline{U}}{\partial y}}_{\text{production}}-\underbrace{\mathscr{D}}_{\text{dissipation}}+\underbrace{\frac{\partial}{\partial y}(J)}_{\text{diffusion}} \quad \text{TKE.} \tag{3}$$

The boundary conditions on the momentum equation are

$$y=0, \quad \left\{\begin{matrix}\overline{U}=0,\\ \overline{V}=0,\end{matrix}\right\} \quad \lim_{y\to\infty}\overline{U}=U_\infty. \tag{4}$$

The equation for TKE is not solved all the way to the wall in STAN5, but only to $y^+ = 2A^+$, where A^+ is a measure of sublayer thickness. It is assumed that the flow is in local equilibrium (experiments confirm this assumption) below $y^+ = 2A^+$, and Prandtl's mixing length can be used in this region. The TKE at this point is calculated such that at $y^+ = 2A^+$ the eddy viscosity obtained from the mixing-length model is equal to the one obtained from a one-equation model of turbulence. This condition gives the following boundary conditions on TKE:

$$\left.\begin{aligned}\frac{q^2}{2}&=\left(\frac{\kappa}{A_q}l\frac{\partial \overline{U}}{\partial y}\right) \quad \text{at} \quad y^+=2A^+,\\ \lim_{y\to\infty}\frac{q^2}{2}&=\frac{q_\infty^2}{2}.\end{aligned}\right\} \tag{5}$$

Here κ is the von Kármán constant; $\kappa = 0{\cdot}41$.

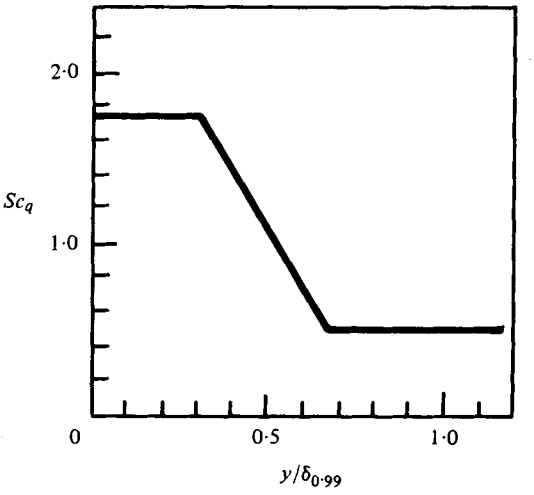

FIGURE 2. Variation of turbulent Schmidt number through the boundary layer, as assumed in this model.

The following terms must be modelled in (2) and (3) in order to obtain a solvable set of equations: $\overline{u'v'}$, $\mathscr{D}$, J. The term for $\overline{u'v'}$ will be modelled after Boussinesq (1877) with an eddy-viscosity model:

$$-\overline{u'v'} = \epsilon_M \frac{\partial \bar{U}}{\partial y}. \tag{6}$$

The eddy diffusivity for momentum, ϵ_M, will be modelled after Prandtl (1945) and Kolmogorov (1942):

$$\epsilon_M = \frac{A_q}{\kappa} l \left(\frac{q^2}{2}\right)^{\frac{1}{2}}. \tag{7}$$

The term $\mathscr{D}$, dissipation of TKE, will be modelled as given in Launder & Spalding (1972):

$$\mathscr{D} = \rho B_q \kappa \frac{(\frac{1}{2}q^2)^{\frac{3}{2}}}{l}. \tag{8}$$

The diffusion of TKE J is also to be modelled as in Launder & Spalding (1972):

$$J = \rho(\nu + \epsilon_q) \frac{\partial(\frac{1}{2}q^2)}{\partial y} \tag{9}$$

using $Sc_q = \epsilon_M/\epsilon_q$. The production of TKE, $\mathscr{P}$, can be expressed as

$$\mathscr{P} = -\rho\overline{u'v'}\frac{\partial U}{\partial y} = \rho\left(\frac{A_q}{\kappa}\right) l \left(\frac{q^2}{2}\right)^{\frac{1}{2}} \left(\frac{\partial \bar{U}}{\partial y}\right)^2. \tag{10}$$

To complete the model, the following constants or functions need to be specified: l, A_q, B_q, Sc_q. The term A_q is the production constant and can be obtained from the value of the stress energy ratio, $-\overline{u'v'}/q^2$, near the wall; it is generally about 0·22 (Wolfstein 1969). The dissipation constant B_q can be evaluated under the condition that the production of TKE is equal to its dissipation in the region near the wall. This condition gives the following relation:

$$B_q = \frac{A_q^3}{\kappa^4}, \quad \kappa = 0{\cdot}41. \tag{11), (12}$$

From the above equations, $B_q = 0{\cdot}377$ is obtained.

The Schmidt number of TKE, Sc_q, is expressed as is shown in figure 2. It has a value of 1·75 near the wall and 0·5 near the free stream. Launder & Spalding (1972) suggest that for film-cooling applications Sc_q should follow a linear distribution from 1·75 near the wall down to 0·5 near free stream; however, during the present predictions, the distribution shown in the preceding figure was found to work better. The extended region of $Sc_q = 0{\cdot}5$ near free stream played an important role in modeling the correct diffusion of TKE near the edge of the momentum boundary layer. The value near the wall did not seem to be as important because of the dominant role of production and dissipation in this region.

The last quantity to be modelled to complete the set is the mixing length, l. Predictions and data show that all other constants mentioned above have their usual values (i.e. the values used for two-dimensional flat-plate boundary predictions). The success of predictions depended very strongly on the correct modelling of l, as will be shown and discussed in the following sections.

2.2. *Mixing-length model*

The two-layer mixing-length model presented here was developed specifically for the recovery region, but should also be applicable (with some modification) to the full-coverage region. The full-coverage boundary layer should behave almost like a recovery region between the injection rows.

The following requirements should be met by a mixing-length model for it to have at least some limited universality:

(*a*) It should be possible to relate the deviations from the two-dimensional mixing length to physical events taking place in the flow field.

(*b*) The dynamics of the model should allow it to relax back to a two-dimensional flat-plate mixing length after the blowing region.

The general approach taken in modelling the mixing length will be described in the following sections. First the flow structure in the recovery region will be discussed. Then each region in the mixing-length profiles will be discussed, and the empirical equations will be given, with supporting physical arguments. Figures 1 (*a*, *b*) show the mixing-length distributions obtained from the experiments (Yavuzkurt *et al.* 1977) by

$$l = \frac{(-\overline{u'v'})^{\frac{1}{2}}}{\partial \bar{U}/\partial y} \tag{13}$$

for two blowing ratios, $M = 0{\cdot}4$ and $M = 0{\cdot}9$.

2.2.1. *Flow structure in the recovery region.* Figure 3 represents the flow in the recovery region interpreted as a dual layer. The basic structure is that of a new two-dimensional boundary layer growing inside the old, thick boundary layer. The thickness of the inner boundary layer is δ', and the thickness of the overall boundary layer (thickened by the injection process in the full-coverage region) is δ. In the middle regions the two boundary layers blend (the cross-hatched area) with the help of cumulative jet spread. The region next to the wall is not cross-hatched, however, because the processes in this region are completely controlled by the wall. The two-dimensional internal boundary layer has an initial thickness at the start of the recovery region which depends on the upstream conditions (e.g. the blowing ratio). This internal boundary-layer growth has been observed by several other experimenters whenever

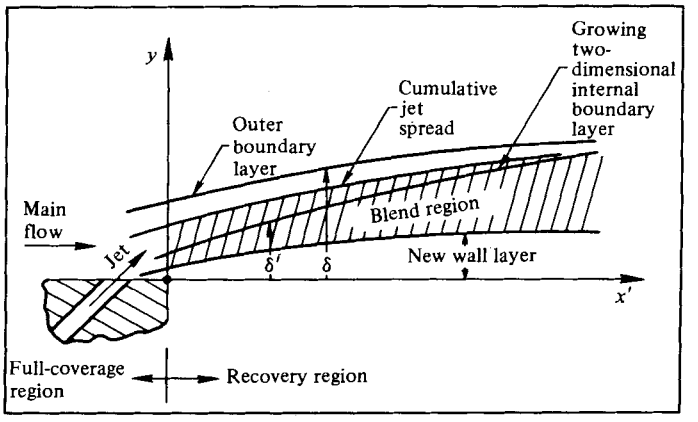

FIGURE 3. Flow structure in the recovery region.

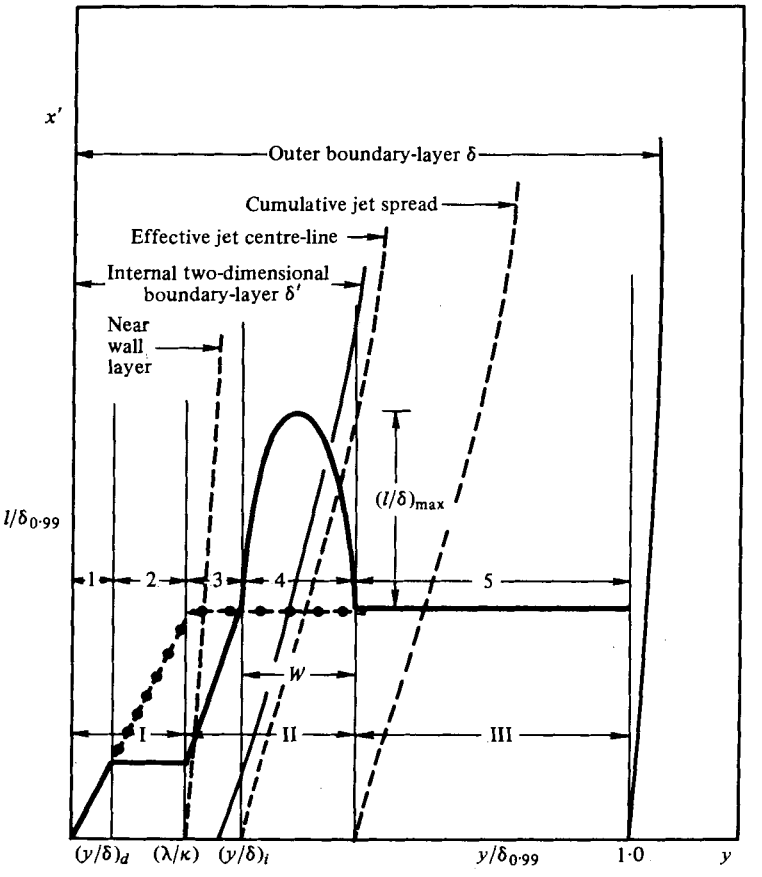

FIGURE 4. Mixing-length model and flow structure in the recovery region.
-●-●-●-, two-dimensional mixing length; ——, modelled mixing length.

there is a sudden change of the surface conditions. For example, Antonia & Luxton (1972) observed such an internal boundary layer in their experiments on the response of a turbulent boundary layer to a step change in surface roughness.

When the measured mixing-length profiles in figures 1(*a*, *b*) are examined in the light of this model, five distinguishable mixing-length regions can be identified, numbered in figure 4. In that same figure, the three distinguishable flow regions are shown, labelled I, II, and III. Region I is the near-wall region of the two-dimensional internal boundary layer; region II is the blend region dominated by cumulative jet effects; and region III is the outer region, dominated by the outer region of the thick boundary layer.

2.2.2. *Region* 1 *of the mixing length.* The innermost region, very close to the wall where $l = \kappa y$, is termed region 1. Experiments show that this region extends up to $y/\delta \simeq 0{\cdot}14$ for $M = 0{\cdot}4$, but only up to $y/\delta \simeq 0{\cdot}055$ for $M = 0{\cdot}9$.

This is the inner region of the new two-dimensional internal boundary layer where the length scale is based on the distance from the wall, y. For programming convenience, the mixing length and the distance from the wall in all the regions were normalized on the total boundary layer of thickness δ. In this region, however, the wall effects are dominant and determine the heat transfer regardless of the blowing ratio. The effect of blowing is mainly to change the initial thickness of the internal two-dimensional boundary layer. The proposed model for this region is:

$$\left(\frac{l}{\delta}\right) = \kappa\left(\frac{y}{\delta}\right) D \quad \text{for} \quad 0 < \left(\frac{y}{\delta}\right) \leqslant \left(\frac{y}{\delta}\right)_d, \tag{14}$$

where D is the damping function (Van Driest) and $(y/\delta)_d$ is the departure point from the κy line. This point corresponds to $y/\delta' = \lambda/\kappa$ for the inner two-dimensional boundary layer of thickness δ'.

The following empirical equation is given for $(y/\delta)_d$:

$$\left(\frac{y}{\delta}\right)_d = \frac{\lambda}{\kappa} + C_1 M\left[\left(\frac{x'}{\delta}\right) - C_2\right], \tag{15}$$

where $C_1 = 0{\cdot}0045$ and $C_2 = 37$, and λ is the outer region mixing-length proportionality constant, $\lambda = 0{\cdot}085$. It is seen that as M gets large the initial value of

$$(y/\delta)_d = \lambda/\kappa - C_1 C_2 M$$

gets smaller, indicating that a higher blowing ratio destroys the near-wall layer, causing a smaller initial thickness for the internal boundary layer. This fits the physical situation very well. The constant C_2 is the number of boundary-layer thicknesses at which $(y/\delta)_d$ reaches the λ/κ point for the outer boundary layer. In fact, then, the recovery is completed. (Antonia (private communication) also supports C_2 being 37.) The constant C_1 controls the rate of recovery of the $(y/\delta)_d$ point.

2.2.3. *Region* 2 *of the mixing length.* Experiments show that in this region the mixing length is constant and low, compared to the outer region of a two-dimensional flat-plate boundary layer of the same thickness. This region is barely visible for $M = 0{\cdot}4$ but is obvious for $M = 0{\cdot}9$. It extends up to about $y/\delta = 0{\cdot}2$ for all stations and corresponds to the outer region of the inner boundary layer, where $l = \lambda\delta'$. Here the eddy size does not depend on the distance from the wall, nor does it depend on the total thickness of the outer boundary layer.

The distance of this region from the outer edge means that the outer length scale does not affect it. This region does not extend all the way up to $y = \delta'$ for the reasons stated below.

The following empirical equation is proposed:

$$l = \kappa \left(\frac{y}{\delta}\right)_d \quad \text{for} \quad \left(\frac{y}{\delta}\right)_d < \left(\frac{y}{\delta}\right) \leqslant \frac{\lambda}{\kappa}. \tag{16}$$

This region does not extend all the way up to δ'. As soon as the edge of the inner layer of the outer boundary layer ($y/\delta = \lambda/\kappa$) is encountered, the length scale begins to be affected by the outer length scale of the outer boundary layer. The branch point is given as λ/κ.

2.2.4. *Region 3 of the mixing length.* Experiments show that in this region the mixing length is still below a two-dimensional flat-plate value. This is also barely visible for $M = 0{\cdot}4$ but it obvious for $M = 0{\cdot}9$. In this region, the mixing length rises from the value in region 2 to 0·085. The region starts around $y/\delta = \lambda/\kappa = 0{\cdot}2$ and extends up to $y/\delta \simeq 0{\cdot}3$ for $M = 0{\cdot}9$ and $y/\delta \simeq 0{\cdot}25$ for $M = 0{\cdot}4$ for the first station. It moves away from the wall in the recovery region.

This is the first section of the blend region of inner and outer boundary layers (region II in figure 4). Here the length scale changes from the two-dimensional inner-layer value to the value in the outer layer in a medium dominated by the jet-flow regime.

The following empirical equation is given for this region:

$$\left(\frac{l}{\delta}\right) = a\left(\frac{y}{\delta}\right) + b \quad \text{for} \quad \frac{\lambda}{\kappa} < \left(\frac{y}{\delta}\right) \leqslant \left(\frac{y}{\delta}\right)_i. \tag{17}$$

The linear combination is all that is justified and fits the experiments. Here, $(y/\delta)_i$ is the intersection point of the new mixing-length line and the $l/\delta = \lambda$ line. The $(y/\delta)_i$ point is the effective centre-line of rising jets and moves out in the recovery region as the jets spread outwards. This will later be shown quantitatively in § 2.4.2. The following empirical equation is given for this point:

$$\left(\frac{y}{\delta}\right)_i = \frac{\lambda}{\kappa} + C_3 M\left[\left(\frac{x'}{\delta}\right) + C_4\right]. \tag{18}$$

It has an initial value of $\lambda/\kappa + C_3 C_4 M$ and an advance rate of $C_3 M(x'/\delta)$ in the downstream direction. The initial value increases with M, indicating a deeper penetration for high blowing, which fits the physics. The values of the constants are

$$C_3 = 0{\cdot}0275, \quad C_4 = 4{\cdot}0 \tag{19}$$

and the equations for coefficients a and b in (17) are

$$a = \frac{\lambda - \kappa(y/\delta)_d}{(y/\delta)_i - \lambda/\kappa}, \tag{20}$$

$$b = \frac{-\lambda^2/\kappa + \kappa(y/\delta)_d\,(y/\delta)_i}{(y/\delta)_i - \lambda/\kappa}. \tag{21}$$

2.2.5. *Region 4 of the mixing length.* Experiments show that a region of augmented mixing length is located between $0{\cdot}24 \leqslant y/\delta < 0{\cdot}37$ for $M = 0{\cdot}4$ and between $0{\cdot}35 \leqslant y/\delta < 0{\cdot}55$ for $M = 0{\cdot}9$ at the start of the recovery region. This region is wider

and higher for $M = 0{\cdot}9$ than for $M = 0{\cdot}4$. The augmented region vanishes in the recovery regions.

The augmentation in the mixing length occurs owing to high shear between the cumulative jet spread and the outer layer fluid. The maximum in the augmentation occurs somewhere between the outer edge of the jet spread and the effective jet centre-line. In the case of higher blowing, this region is moved outwards because of the greater jet penetration. The augmented region also moves outwards in the downstream direction in the recovery region, as jets rise; but at the same time it vanishes, as there is a decrease in shear between the cumulative jet spread and the outer layer. This is discussed further in Yavuzkurt *et al.* 1977).

This region was modelled as a parabola, the simplest curve which fits the data:

$$\left(\frac{l}{\delta}\right)_a = c\left(\frac{y}{\delta}\right)^2 + d\left(\frac{y}{\delta}\right) + e \tag{22}$$

and

$$\left(\frac{l}{\delta}\right) = \lambda + \left(\frac{l}{\delta}\right)_a \quad \text{for} \quad \left(\frac{y}{\delta}\right)_i < \left(\frac{y}{\delta}\right) \leqslant \left(\frac{y}{\delta}\right) + W. \tag{23}$$

Here, c, d and e are constant coefficients; their values depend on end points and will be given after the discussion of the end points. The quantity W is the width of the augmented region at the $l/\delta = \lambda$ level. Based on the experimental evidence, it was made a function of blowing ratio M. Since no better formulation was possible, it was expressed as a linear function

$$W = C_7 M. \tag{24}$$

In figure 4, $(l/\delta)_{\max}$ is the maximum value of the augmentation. Its decay in the downstream direction was expressed as an exponential function:

$$\left(\frac{l}{\delta}\right)_{\max} = \left(\frac{l}{\delta}\right)_{\max,\,i} \exp\left(-\frac{(x'/\delta)}{C_6}\right); \tag{25}$$

$(l/\delta)_{\max,\,i}$ is the initial value of augmentation. It is given from the experimental evidence, as follows:

$$\left(\frac{l}{\delta}\right)_{\max,\,i} = C_5 M. \tag{26}$$

The coefficients for the parabola are given as

$$c = \frac{4(l/\delta)_{\max}}{W^2}, \tag{27}$$

$$d = \frac{8(l/\delta)_{\max}}{W^2}\left[\left(\frac{y}{\delta}\right)_i + \frac{W}{2}\right], \tag{28}$$

$$e = -\frac{4(l/\delta)_{\max}}{W^2}\left(\frac{y}{\delta}\right)_i\left[\left(\frac{y}{\delta}\right)_i + W\right]. \tag{29}$$

The values of the constants are

$$C_5 = 0{\cdot}496, \quad C_6 = 0{\cdot}435, \quad C_7 = 0{\cdot}333. \tag{30}$$

2.2.6. *Region 5 of the mixing length.* Experiments show that in this region the length scale is constant, and it is $l/\delta = \lambda \cong 0{\cdot}085$. The region begins after the augmented region and continues up to the free stream for both blowing ratios.

This region is the outer layer of the outer boundary layer, where the mixing length scales on the total thickness δ. In this region, the following empirical equation is given:

$$\left(\frac{l}{\delta}\right) = \lambda \quad \text{for} \quad \left(\frac{y}{\delta}\right)_i + W < \left(\frac{y}{\delta}\right). \tag{31}$$

2.2.7. *Comments on the mixing-length model.* Except for the usual universal values of $\kappa = 0{\cdot}41$ and $\lambda = 0{\cdot}085$, seven constants were used to model the mixing length. The number of constants looks very large at first glance, but when examined more closely one can see that this number is reasonable. Three different flow structures are being modelled: inner and outer boundary layers and blend region in between, as well as their dynamics in the streamwise direction.

During the prediction process it was observed that the most important constants in the mixing-length model were C_1, C_2, C_3 and C_4. The constants used to specify the augmented region (C_5, C_6 and C_7) did not prove significant. The augmented region did not have much effect on the predictions because it lies in the outer region of the boundary layer. It also decays rapidly. During computer experiments with W and $(l/\delta)_{\max}$, changing the values of C_5 and C_7 did not affect the results at all. It is possible that the augmented region can be completely eliminated for the recovery region predictions, thus reducing the number of constants to four. The constants were obtained from the empirical data rather than from computer experiments. Kacker & Whitelaw (1970) used five constants to model the mixing length for prediction of wall jet and wall-wake flows, which are similar to, but not more complicated than, the recovery region of the present full-coverage film-cooled surface. In the present model the augmented region is kept for convenience and for easy adaptation of this mixing-length model to the full-coverage region where the peak of augmentation moves closer to the wall and is important for the prediction of heat transfer.

In the recovery region predictions, especially for $M = 0{\cdot}9$, the most important region of the mixing length, turned out to be the reduced mixing-length region near the wall. Without correct modelling of this region, predictions always failed. The first four constants are the important ones in the recovery region predictions.

It was observed that only regions 2, 3 and 4 show deviations from a usual two-dimensional mixing-length model. Region 2 proved especially interesting, because it had been thought that the jet mainstream interaction would increase the mixing length above the two-dimensional value (Choe *et al.* 1975; Crawford *et al.* 1976). Choe *et al.* and Crawford *et al.* calculated the mixing length for low blowing and in the full-coverage region. They observed that the augmented region (region 4) moved closer to the wall and did not observe regions 2 and 3, which are more easily observable for high blowing. In reality, regions 2 and 3 are very important in predictions, as is explained in § 2.3.1.

The relaxation to the two-dimensional state takes place in the following manner. As the cumulative effects of jets move downstream and diffuse out, they lose their strength and the augmentation dies out ($\sim 3\delta$ or 4δ), but the effective centre-line of the jets, the $(y/\delta)_i$ point, continues to rise. At the same time the inner boundary-layer thickness δ' grows faster than δ (δ almost stops growing after the injection stops), and finally, when they merge (in approximately 40δ), the recovery process is complete.

2.2.8. *Comparison of measured and modelled mixing lengths.* It is important to establish that the heuristic model assembled in the preceding paragraphs does in fact

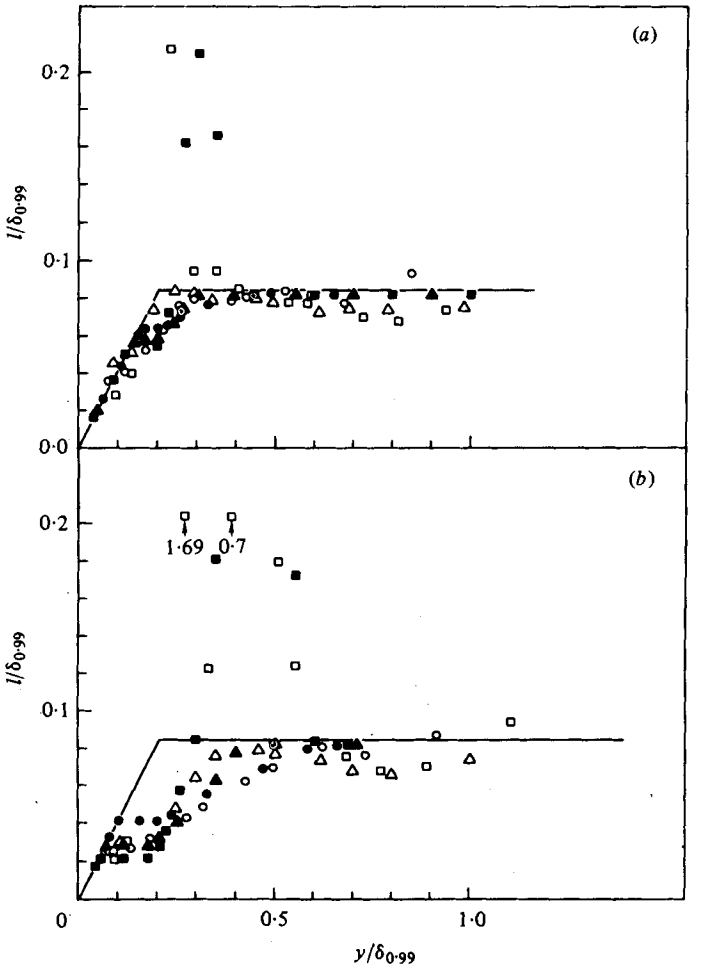

FIGURE 5. Comparisons of the piecewise mixing-length model and the data in the recovery region. (*a*) $M = 0{\cdot}4$. (*b*) $M = 0{\cdot}9$.——, flat plate. Solid symbols are for the model, open symbols are used for the data. □, $x = 188$; △, $x = 214$; ○, $x = 256$.

reflect the behaviour of the mixing length derived directly from the experiments. Figure 5 compares the piecewise mixing-length model with the data already presented in figure 1. Results are shown both for $M = 0{\cdot}4$ and $M = 0{\cdot}9$, with the model always being represented by the solid symbols and the data always by the open symbols. It is evident from inspection of figure 5 that the proposed model captures the principal features of the mixing-length distribution and its variation both with blowing and with streamwise distance. It next remains to compare the consequences of using this mixing-length distribution with the experimental evidence for mean velocity and turbulence kinetic energy distributions.

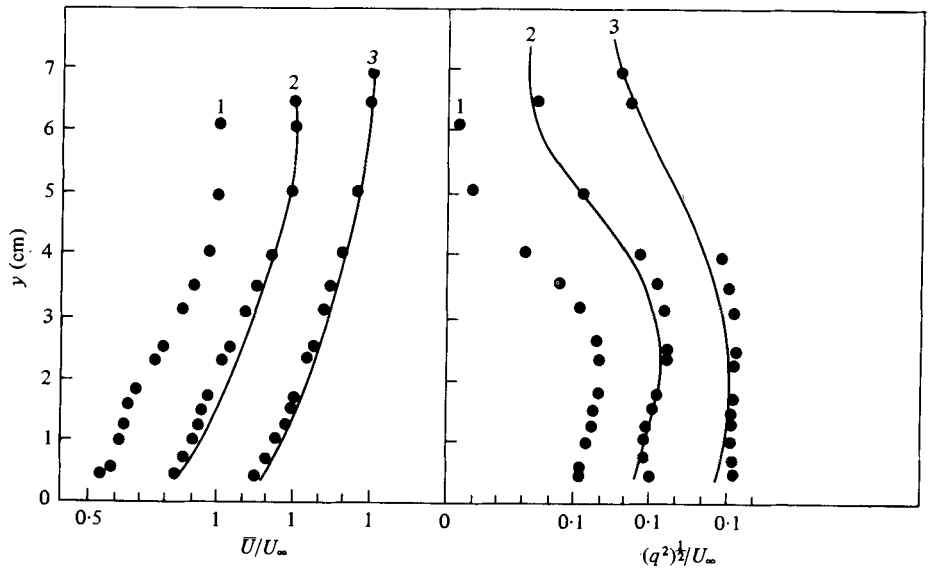

FIGURE 6. Predictions of streamwise mean velocity component, $\bar{U}$, and turbulent kinetic energy, q^2, for $M = 0{\cdot}4$. ——, prediction; ●, data. 1, Start of recovery (initial profiles). 2, Recovery region, 11th plate. 3, Recovery region, 27th plate.

3. Predictions

The mixing-length model, together with the TKE equation, was used as a one-equation model of turbulence in the two-dimensional boundary-layer program STAN5 (Crawford & Kays 1975). Starting with the spanwise-averaged mean velocity and TKE profiles at the beginning of the recovery region ($x = 188$ cm), very successful predictions of TKE and the mean velocity profiles for $M = 0{\cdot}4$ and $M = 0{\cdot}9$ were obtained at two downstream stations in the recovery region ($x = 214$ cm, 256 cm).

Figure 6 shows a comparison of the predicted mean velocity and TKE profiles with the experimental data for $M = 0{\cdot}4$ on the two stations in the recovery region, starting with the spanwise-averaged initial profiles. The prediction of mean velocity on plate 11 ($x = 214$ cm) is somewhat high in the middle region of the boundary layer, but the difference lessens by the 27th plate ($x = 256$ cm). For TKE profiles, the predictions are somewhat low. These figures show that the model predicts a slightly faster recovery to the two-dimensional state than the physical process, but the difference is not that great. The reason for lower TKE predictions might be the mixing length. In figure 5 the mixing-length model for $M = 0{\cdot}4$ is slightly low, compared to measurements, in the region $0{\cdot}15 < y/\delta < 0{\cdot}3$. This means that the model results in a smaller production and a higher dissipation than the reality, yielding lower TKE values compared to the experiment.

Figure 7 shows a comparison of the mean velocity and TKE profiles with the experimental data for $M = 0{\cdot}9$ on the two stations in the recovery region, starting with the spanwise-averaged initial profiles. The suggested model predicts the $M = 0{\cdot}4$ case well, and the predictions for the $M = 0{\cdot}9$ case are excellent. It is important to remember that the constants do not change with the blowing ratio. Both cases were predicted with the same set of constants for the mixing length. The other constants in the one-

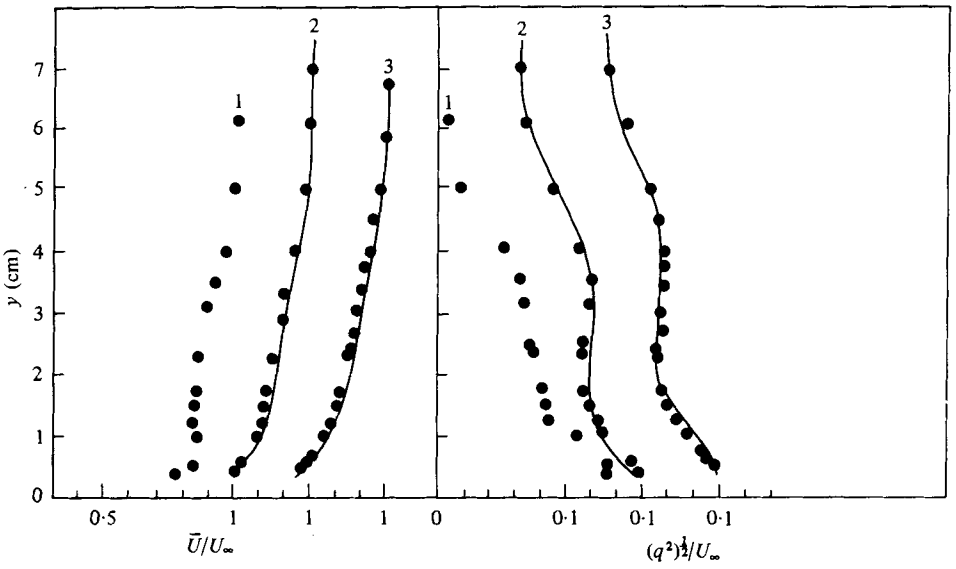

FIGURE 7. Predictions of streamwise mean velocity component, $\bar{U}$, and turbulent kinetic energy, q^2, for $M = 0{\cdot}9$. ——, prediction; ●, data. 1, Start of recovery (initial profiles). 2, Recovery region, 11th plate. 3, Recovery region, 27th plate.

equation model are the usual ones employed for two-dimensional boundary-layer predictions. The authors believe that the model will successfully predict blowing ratios up to $M = 1{\cdot}0$. Further extrapolation of the model might be dangerous due to the changing hydrodynamic character of the flows.

The importance of accounting for the reduced mixing near the wall, when making predictions in the recovery region, is demonstrated by figure 8. This figure compares the experimental data with the predictions of TKE (in the recovery region on the 27th plate for $M = 0{\cdot}9$). Predictions were made with two different mixing-length models: one of them is the normal two-dimensional flat-plate mixing length, and the other is the model developed in this study, which results in a smaller value near the wall. The new model predicts perfectly, whereas the usual two-dimensional mixing length predicts much higher TKEs almost up to the first half of the boundary layer. The reason lies in the relationship between the mixing length and the production and dissipation of TKE. Higher mixing lengths increase the production and reduce the dissipation, giving rise to higher TKEs.

The reduced mixing region did not have a significant effect on near-wall velocity profiles; however, it *is* important in heat transfer behaviour because of its influence on the turbulence level.

4. Rationalizing the model

The empirical curve fits already described do in fact match the boundary layer behaviour. The physical arguments are plausible and suggest that the empirical relations could be replaced (if desired) by more conventional forms. In this section some possible alternative equations are examined – without changing the physical

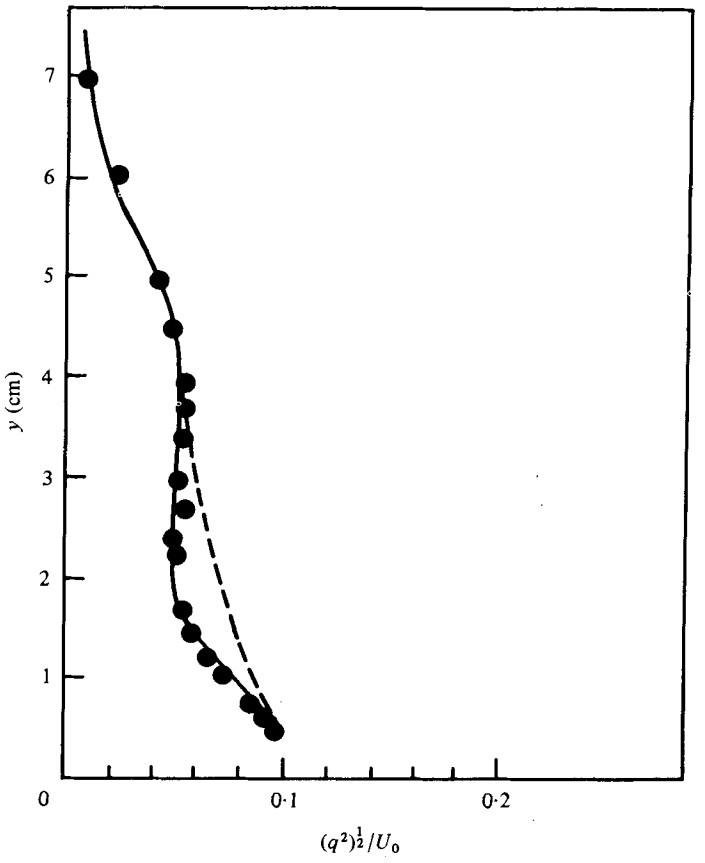

FIGURE 8. Effect of mixing length on predictions of turbulent kinetic energy; $M = 0{\cdot}9$, recovery region, 27th plate. ●, data. Predictions: ——, present model; – – –, two-dimensional flat-plate mixing length.

arguments – both for the purpose of testing the physical argument for reasonableness of the magnitudes and to take advantage of established forms where possible.

4.1. *The outer edge of the inner boundary layer*

The equation governing the thickness of the inner layer is

$$\left(\frac{y}{\delta}\right)_d = \frac{\lambda}{\kappa} + 0{\cdot}0045M\left[\left(\frac{x'}{\delta}\right) - 37\right]. \tag{15}$$

Using a conventional equation for two-dimensional turbulent boundary-layer growth to describe the growth of the internal boundary layer (Schlichting 1968) yields

$$\frac{\delta'}{(x+x'_0)} = 0{\cdot}37\left(\frac{\rho\overline{U}(x+x'_0)}{\mu}\right)^{-\frac{1}{5}}. \tag{33}$$

δ' and $(y/\delta)_d$ are related as follows:

$$\frac{y}{\delta'} = \frac{\lambda}{\kappa} \quad \text{at} \quad \left(\frac{y}{\delta}\right)_d. \tag{34}$$

		x'/δ)		
		0	~5	~12
		δ'(m)		
M				
0·4	Piecewise model	0·028	0·036	0·045
	Boundary-layer formula	0·028	0·033	0·040
0·9	Piecewise model	0·011	0·018	0·028
	Boundary-layer formula	0·011	0·017	0·025

TABLE 1

Therefore,
$$\frac{(y/\delta)_d}{(y/\delta')} = \frac{(y/\delta)_d}{(\lambda/\kappa)} \tag{35}$$

or
$$\frac{\delta'}{\delta} = \frac{(y/\delta)_d}{(\lambda/\kappa)}. \tag{36}$$

Consequently, if one knows the initial value of δ and $(y/\delta)_d$ at $x' = 0$, then the initial δ' can be calculated and x'_0 determined from the formula. After x'_0 is found, the rest of δ' and $(y/\delta)_d$ can be obtained from the boundary-layer growth formula.

In equation (33) the value of U_∞ can be used for the value of $\overline{U}$ since $\overline{U}$ at $\delta'_{0.99}$ is never far from U_∞. For example, for $M = 0{\cdot}9$ the velocity profile is so flat that near $\delta'_{0.99}$
$$\overline{U} \sim U_\infty.$$

For $M = 0{\cdot}4$ the initial thickness of this boundary layer is large (because there is less disturbance), and again around $y \sim \delta'$, $\overline{U} \sim U_\infty$. One might question the use of (33) to predict the growth of the inner layer, since it neglects the effect of the turbulence of the outer regions. It seems justified, however, because around δ' the turbulence levels are quite small for both cases studied here (3–5 %).

By using $\overline{U} \simeq U_\infty = 16{\cdot}7\,\mathrm{m\,s^{-1}}$, $\rho = 1{\cdot}2\,\mathrm{kg\,m^{-3}}$, $\mu = 0{\cdot}9 \times 10^{-5}\,\mathrm{kg\,m^{-1}\,s^{-1}}$, the virtual origin of the internal boundary layer can be calculated for both cases from the initial value of $(y/\delta)_d$. The following values were obtained:

$$\text{for} \quad M = 0{\cdot}4, \quad x'_0 = 1{\cdot}29\,\mathrm{m};$$
$$\text{for} \quad M = 0{\cdot}9, \quad x'_0 = 0{\cdot}41\,\mathrm{m}.$$

The value of $(x'_0)_{M=0.4}$ is greater than $(x'_0)_{M=0.9}$, which is normal because, for low blowing, the undisturbed region near the wall is larger. After calculation of virtual origins, the comparisons shown in table 1 were obtained between the piecewise model and the internal boundary-layer growth formula. As is seen from the comparison, the present linear model and the boundary-layer growth results compare quite well. In fact, when one looks at the data, the boundary-layer formula seems to be closer.

The following changes can be suggested in the present model. Instead of calculating $(y/\delta)_d$ from the piecewise linear formula (15), $(y/\delta)_{d,\,\mathrm{initial}}$ can be calculated, which involves only one empirical constant. Then, using

$$\frac{\delta'_{\mathrm{initial}}}{\delta} = \frac{(y/\delta)_{d,\,\mathrm{initial}}}{(\lambda/\kappa)}, \tag{37}$$

		(x'/δ)		
		0	~5	~12
		δ' (m)		
M				
0·4	Piecewise model	0·244	0·3	0·37
	Jet-spread formula	0·244	0·3	0·333
0·9	Piecewise model	0·3	0·424	0·59
	Jet-spread formula	0·3	0·55	0·67

TABLE 2

δ'_{initial} can be found, and $$x'_0 = \left[\frac{\delta'_{\text{initial}}}{0{\cdot}37(\rho U_\infty/\mu)^{-\frac{1}{5}}}\right]^{\frac{5}{4}}. \tag{38}$$

Other δ' can be calculated as follows:

$$\delta' = (x' + x'_0)\, 0{\cdot}37 \left(\frac{\rho \bar{U}(x' + x'_0)}{\mu}\right)^{-\frac{1}{5}} \tag{39}$$

and $$\left(\frac{y}{\delta}\right)_d = \left(\frac{\lambda}{\kappa}\right)\left(\frac{\delta'}{\delta}\right). \tag{40}$$

Here, even though the equation for boundary-layer growth is still empirical, it is more universal than the constant supplied in the formula for $(y/\delta)_d$. So the $(y/\delta)_d$ formula can be reduced to one empirical constant supplied by the present experiments and a more universally accepted empirical equation.

4.2. *Comparison of the development of the $(y/\delta)_i$ point with jet spreading theory*

It is argued that the dynamics of the $(y/\delta)_i$ point corresponds to the rising of the effective jet centre-line. In this section, the output of the empirical equation for $(y/\delta)_i$ (equation (18)) is compared with the results of an equation describing the rising of the centre-line of a jet in crossflow (Abramovich 1960):

$$\left(\frac{x' + x''_0}{D}\right) = \left(\frac{1}{M^2}\right)^{1{\cdot}3}\left(\frac{y}{D}\right)^3 + \left(\frac{y}{D}\right)\cot\alpha'. \tag{41}$$

Here x''_0 is the virtual origin for the effective jet action, D is the diameter of a single jet, and α' is the injection angle. The solution of this equation depends on four parameters: x''_0, D, M and α'. The last three are supplied by the problem physics, and the only unknown is the virtual origin, which can be calculated from the empirical input, i.e. from the initial value of $(y/\delta)_i$, assuming that effective jet spread occurs according to the equation (41).

The results of the virtual origin calculation are:

$$\text{for} \quad M = 0{\cdot}4, \quad x''_0 = 0{\cdot}13\,\text{m};$$

$$\text{for} \quad M = 0{\cdot}9, \quad x''_0 = 0{\cdot}055\,\text{m}.$$

Then, with these results and from (41), the spreading of the jets can be calculated and compared with the present model values of $(y/\delta)_i$. The results are shown in table 2. As is seen again, the comparison is not bad. This supports the argument that $(y/\delta)_i$ point moves out with distance similar to the jet centre-line.

The following changes can be made in the model to replace the constant C_3 with the more accepted empirical equation; or with this physically supporting agreement, the old model for $(y/\delta)_i$ can be left as it is. The change is as follows. Calculate

$$\left(\frac{y}{\delta}\right)_{i,\,\text{initial}} = \frac{\lambda}{\kappa} + C_3 C_4 M. \tag{42}$$

Then

$$y_{\text{initial}} = \delta \left(\frac{y}{\delta}\right)_{i,\,\text{initial}}. \tag{43}$$

Calculate x_0'' from

$$\frac{x_0''}{D} = \left(\frac{1}{M^2}\right)^{1\cdot3} \left(\frac{y_{\text{initial}}}{D}\right)^3 + \frac{y_{\text{initial}}}{D} \cot \alpha'. \tag{44}$$

Then calculate new y_i's from (41).

4.3. *Other changes suggested*

To include the effect of P/D (pitch-to-diameter ratio), the blowing ratio M in the formulae can be replaced by

$$F = M\left(\frac{\pi D^2}{4P^2}\right)$$

or by

$$F' = M^2\left(\frac{\pi D^2}{4P^2}\right).$$

Here F' reflects the relative effects of the jet and free-stream momentum. It is thought that it will be better to replace M by F'; by inclusion of an empirical jet-spread equation, the variation in the injection angle (α') could also be represented in the model.

5. Summary of important points

The important points in this work can be summarized as follows.

(*a*) The flow in the recovery region can be described in terms of a two-layer model: an outer boundary layer where the length-scale scales on the total thickness of the layer, and an inner layer where the mixing length is the usual κy and $\lambda\delta$. The two layers blend into each other with the spreading of jets. Recovery to a two-dimensional boundary layer is completed when the inner and outer layers finally merge.

(*b*) A one-equation model of turbulence can be used in a two-dimensional finite-difference boundary-layer computer program to predict the mean velocity and TKE profiles in the recovery region. The one-equation model used here employs the TKE conservation equation with an algebraic relationship for the mixing length. Mixing-length values calculated from the data were input to the program using a piecewise continuous, heuristic fit consistent with the concept of the two quasi-independent layers observed in the recovery region. This mixing-length pattern, used with a set of otherwise normal constants (for two-dimensional boundary-layer predictions), successfully predicted all the spanwise-averaged features of the flow. This strongly suggests that all of the principal mechanisms were modelled adequately by the mixing-length formulation.

(*c*) It has been shown that the piecewise continuous, heuristic model can be replaced by a set of relations taken from the literature describing the spreading of jets and the growth of boundary layers, thus supporting the physical arguments behind the mixing-length model.

This work was sponsored by the National Aeronautics and Space Aministration, Lewis Research Center, under Contract NAS-314336, and by the Scientific and Technical Research Council of Turkey (Türkiye Bilimsel ve Teknik Arastirma Kurumu), which supported the first author (Savas Yavuzkurt) during his stay at Stanford. The authors also wish to thank Dr H. Choe and Dr M. Crawford, whose apparatus was the main frame for the present work and whose careful studies led to this one.

REFERENCES

ABRAMOVICH, G. N. 1960 *The Theory of Turbulent Jets*, p. 544. Massachusetts Institute of Technology Press.

ANTONIA, R. A. & LUXTON, R. E. 1972 The response of a turbulent boundary layer to a step change in surface roughness. Part 2. Rough to smooth. *J. Fluid Mech.* **53**, 737–757.

BOUSSINESQ, J. 1877 Théorie de l'écoulement tourbillant. *Mém. prés. div. Sav. Acad Sci· Inst. Fr.* **23**, Paris.

CHOE, H., KAYS, W. M. & MOFFAT, R. J. 1975 Turbulent boundary layer on a full-coverage film-cooled surface – An experimental heat transfer study with normal injection. *N.A.S.A. Rep.* CR-2642. (Also *Stanford Univ., Mech. Engng Dept Rep.* HMT-22.)

CRAWFORD, M. E. & KAYS, W. M. 1975 STAN5 – A program for numerical computation of two-dimensional internal/external boundary-layer flows. *Stanford Univ., Mech. Engng Dept Rep.* HMT-23.

CRAWFORD, M. E., KAYS, W. M. & MOFFAT, R. J. 1976 Heat transfer to a full-coverage film-cooled surface with 30-deg. slanthole injection. *Stanford Univ., Mech. Engng Dept Rep.* HMT-25.

ERICKSEN, V. L., ECKERT, E. R. G. & GOLDSTEIN, R. J. 1971 A model for analysis of the temperature field downstream of a heated jet injected into an isothermal crossflow at an angle of 90° C, *N.A.S.A. Rep.* CR-72990.

GOLDSTEIN, R. J., ECKERT, E. R. G., ERICKSON, V. L. & RAMSEY, J. W. 1969 Film cooling following injection through inclined circular tubes *N.A.S.A Rep.* CR-73612.

HERRING, H. J. 1975 A method of predicting the behaviour of a turbulent boundary layer with discrete transpiration jets. *Trans. A.S.M.E.* A, *J. Engng Power* **97**, 214–224.

KACKER, S. C. & WHITELAW, J. H. 1970 Prediction of wall-jet and wall-wake flows. *J. Mech. Engng Sci.* **12**, 404–420.

KOLMOGOROV, A. N. 1942 Equations of turbulent motion of an incompressible turbulent fluid. *Izv. Akad. Nauk S.S.S.R., Ser. Phys.* **6**, No. 1–2, 56.

LAUNDER, B. E. & SPALDING, D. B. 1972 *Lectures in Mathematical Models of Turbulence.* Academic.

MAYLE, R. E. & CAMARATA, F. J. 1975 Multihole cooling film effectiveness and heat transfer. *Trans. A.S.M.E.* C, *J. Heat Transfer* **97**, 534–538.

PAI, B. R. & WHITELAW, J. H. 1971 The prediction of wall temperature in the presence of film cooling. *Int. J. Heat Mass Transfer* **14**, 409–426.

PATANKAR, S. V., RASTOGI, A. K. & WHITELAW, J. H. 1973 The effectiveness of three-dimensional film-cooling slots – III. Predictions. *Int. J. Heat Mass Transfer* **16**, 1673–1681.

PRANDTL, L. 1945 Über ein neues Formelsystem für die ausgebildete Turbulenz. *Nachrichten von der Akad. der Wissenschaft in Göttingen.*

SCHLICHTING, H. 1968 *Boundary-Layer Theory*, 6th edn, p. 533. McGraw-Hill.

WOLFSTEIN, M. 1969 The velocity and temperature distribution in one-dimensional flow with turbulence augmentation and pressure gradient. *Int. J. Heat Mass Transfer* **12**, 301–318.

YAVUZKURT, S., MOFFAT, R. J. & KAYS, W. M. 1977 Full-coverage film-cooling: 3-dimensional measurements of turbulence structure and prediction of recovery region hydrodynamics. *Stanford Univ., Mech. Engng Dept Rep.* HMT-27.

YAVUZKURT, S., MOFFAT, R. J. & KAYS, W. M. 1980 Full-coverage film cooling. Part 1. Three-dimensional measurements of turbulence structure. *J. Fluid Mech.* **101**, 129–158.